Research Article

Florence Grenapin, Alessio D'Errico* and Ebrahim Karimi

Spin–orbit coupling induced by ascorbic acid crystals

https://doi.org/10.1515/nanoph-2022-0502
Received August 25, 2022; accepted December 9, 2022;
published online January 16, 2023

Abstract: Some anisotropic materials form semicrystalline structures, called spherulites, when observed in a polarisation microscope, exhibit a characteristic "maltese-cross"-like pattern. While this observation has been hitherto considered as a tool to characterize these materials, we show that these patterns are associated with a strong light's spin–orbit coupling induced by the spherulite structures. We experimentally demonstrate these effects using samples of crystallized ascorbic acid and observing the creation of optical vortices in transmitted laser beams, as well as the formation of inhomogeneous polarisation patterns. Our findings suggest the use of some spherulites based on other materials in frequency ranges, e.g. in the THz domain, where polarisation and spatial shaping of electromagnetic radiation is still a challenging task.

Keywords: metasurfaces; orbital angular momentum; spherulites; structured light.

1 Introduction

Polymer spherulites are spherically symmetric semicrystalline structures typically observed when a molten polymer is slowly cooled down [1]. The slow cooling allows polymer chains to form in ordered configurations. The crystallization starts around point defects and consists of lamellae structures that, in the absence of temperature gradients, grow radially from the defect centre.

***Corresponding author: Alessio D'Errico**, Nexus for Quantum Technologies, University of Ottawa, K1N 5N6, ON, Ottawa, Canada, E-mail: aderrico@uottawa.ca. https://orcid.org/0000-0002-6964-4328
Florence Grenapin, Nexus for Quantum Technologies, University of Ottawa, K1N 5N6, ON, Ottawa, Canada, E-mail: flo.grenazin@gmail.com
Ebrahim Karimi, Nexus for Quantum Technologies, University of Ottawa, K1N 5N6, ON, Ottawa, Canada; and National Research Council of Canada, Ottawa, Canada, E-mail: ekarimi@uottawa.ca. https://orcid.org/0000-0002-8168-7304

The radially directed fibrillar structure can be easily seen at low magnification. Such fibrils are composed of one or multiple crystals elongated in the radial direction. Such media have been the subject of intense research in the last decade due to their effect on optical beams that couples optical polarisation and inhomogeneous phase transformations. As a consequence of the optical anisotropy of the crystals, spherulites can be considered as one of the simplest examples of patterned anisotropic media. More specifically, Pancharatnam–Berry Optical Elements (PBOEs) [2] are slabs of patterned anisotropic materials whose inhomogeneous orientation of the optic axis can be used to structure the phase and polarisation of light in a way that is conditioned by the polarisation of the input beam. The most known and widely used device of this kind is the q-plate, a PBOE with an optic axis that varies linearly with the azimuthal angle [3, 4]. Q-plates have been used as a tool in different areas [5]: from quantum information and simulation [6, 7] to microscopy and surface structuring [8, 9]. Typically, q-plates are based on liquid crystals, in which case their retardation can be finely controlled either thermally [10] or electrically [11]. More recently, q-plates, as well as other PBOEs, based on subwavelength structures have been developed: from nanostructured glasses [12] to plasmonic metasurfaces [13]. Semiconductor microcavities with similar features have been recently demonstrated [14, 15].

Here, we show how slabs of spherulites – specifically how thin layers of ascorbic acid spherulites – also behave like PBOEs with an azimuthal optic axis dependence. Indeed, when observed in the context of polarized light microscopy, i.e. between crossed polarizers, spherulites display "maltese-cross"-like patterns which strongly resemble q-plate patterns with topological charge $q = 1$ (see Figure 1).

In q-plates, the radial optic pattern introduces an azimuthal phase factor to the light transmitted through it, a factor which is associated with a well-defined amount of Orbital Angular Momentum (OAM). Depending on the input polarisation state, one can generate beams with OAM values of ± 2 or induce singular polarisation patterns, e.g. vector vortex beams. This process is called optical spin to orbit coupling. OAM beams, as well as vector vortex beams, may be exploited to encode classical and quantum information

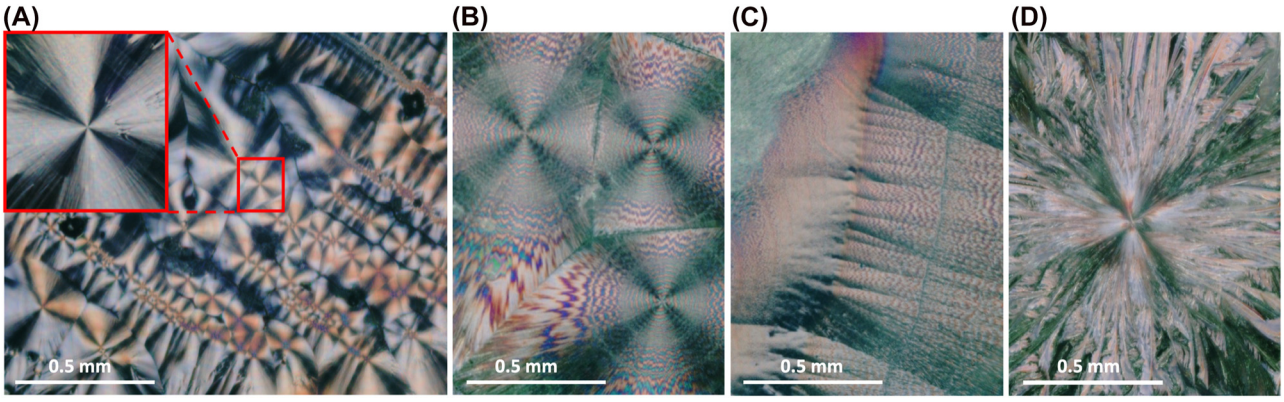

Figure 1: Images of ascorbic acid samples between cross polarizers, illuminated by white light. (A) Sample of ascorbic acid crystals grown at room temperature, from a 10:1 ethanol:water solution. Many "maltese-cross"-like patterns are visible, delimited by boundary regions. In the top left corner, a singled out pattern is enlarged. (B) Sample of ascorbic acid crystals grown at 80 °C, from a pure water solution. The "maltese-cross"-like patterns exhibit a double-banded structure visible as concentric rings of alternating colours. (C) Sample grown in the same conditions as B. Point defects aligned close together on a physical boundary cause a different pattern to arise in the sample. The double-bandedness remains visible, without the cross pattern. (D) Sample of ascorbic acid crystals grown at 120 °C, from a pure water solution. A "maltese-cross"-like pattern is visible, but appears disorganized and coarse. The fibrils themselves are almost recognizable.

[11, 16–20]. Spin–orbit coupling is the basic phenomenon behind the optical spin Hall effect [21, 22].

Spherulite-like structures are observed when evaporating solutions of ascorbic acid dissolved in water (or other solvents, like ethanol). We confirmed our prediction by performing interferometric experiments to ascertain the OAM character of the transmitted beam and spatial Stokes polarimetry to reconstruct the generated polarisation patterns during and after the spherulite formation.

2 Materials and methods

Ascorbic acid ($C_6H_8O_6$), commonly referred to as vitamin C, forms biaxial crystals with monoclinic spheroidal crystal units of $P2_1$ symmetry [23, 24]. The unit cell and indicatrix ellipsoid are shown in Figure 2(A), and the molecular structure of ascorbic acid is shown in Figure 2(C). The molecules themselves are roughly planar and at room temperature growth they are almost strictly oriented in the (010) plane (the plane generated by the axes a and c in Figure 2(A)), the smallest refractive index of the indicatrix is aligned in the b direction.

In our experiment, commercially available ascorbic acid was spread over a slide, dissolved in a solution which was made to evaporate and leave free and dispersed ascorbic acid molecules in the sample. Water and ascorbic acid have great affinity, however, due to its high surface tension, water does not spread out as well on the slide and can take up to a couple hours to dry, at room temperature [25]. The choices of solvent and temperature are important as they determine the thickness of the sample (which affects the retardation), the rate of crystal formation, subtle variations in crystal structure, and the number of molecules present on the slide (whether or not the effects will be visible). Therefore, at first, we chose to dissolve the ascorbic

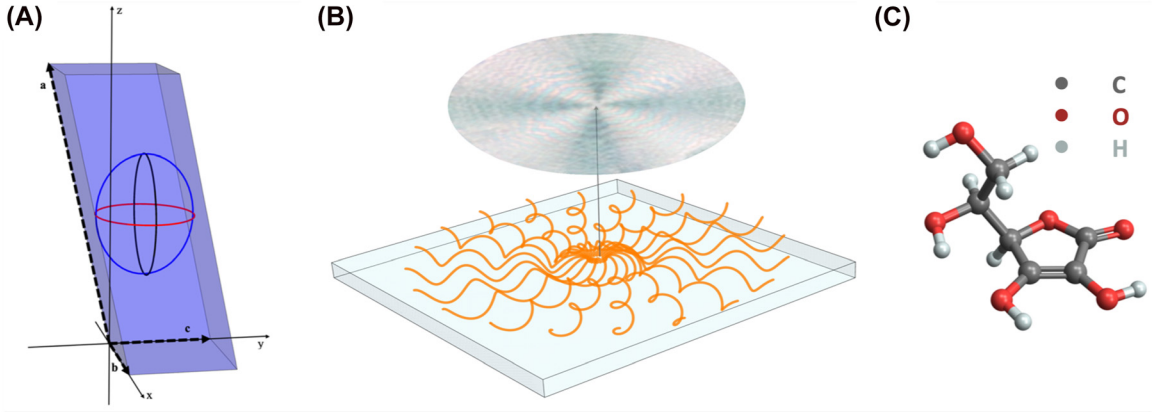

Figure 2: Structure of ascorbic acid spherulites. (A) Schematic of the ascorbic acid crystal unit cell and indicatrix ellipsoid. The three axes of the unit cell are: $a = 17.299(8)$ Å, $b = 6.353(3)$ Å, $c = 6.411(3)$ Å, with $\omega = 102°11'(08')$ the angle between a and c. The three axes of the ellipsoid are: $\alpha = 1.46$, $\beta = 1.6$, $\gamma = 1.75$, with α parallel to b. (B) Twisting of indicatrix ellipsoid along the fibril growth directions. (C) The molecular structure of ascorbic acid. Legend: C, carbon; O, oxygen; H, hydrogen.

acid at room temperature in a solution of 1:10 ethanol:water [26]. On the sample, the spherulite structures formed around point defects from residual powder grains, either accidentally present from undissolved powder grains in the solution or introduced manually after evaporation [25, 27–29]. There is a large variety of patterns that can be observed under different conditions of humidity and temperature [1, 29]. In particular, in specific humidity conditions (relative humidity $RH \approx 30–40\%$) and at room temperature [29], one can observe "maltese-cross"-like patterns when viewing the sample between crossed polarizers and under white light illumination (see Figure 1(A)). Under different conditions, for example at slightly higher temperatures, the crystals can form with a twist, rotating around the fibrillar axis at a certain angle, resulting in a periodic rotation of the indicatrix ellipsoid along the radial direction [30]. This alternation of adjacent regions of relative high and low birefringence forms "banded maltese-cross"-like patterns, where, when viewed under cross-polarizers, regularly spaced concentric rings of alternating brightness appear overtop of the cross-like intensity pattern. In the case of ascorbic acid, "double-banded maltese-cross" patterns form because of the biaxial nature of the rotating ellipsoid [Figure 1(B) and (C)]. By choosing pure water as a solvent which we heated at near boiling point, we observed the double-banded patterns more clearly. In more extreme conditions at higher temperatures, the spherulite patterns become coarse and less organized (see Figure 1(D)).

3 Results

In order to understand the action of ascorbic acid crystals on a light beam around point defects we can adopt the model of a wave retarder with an inhomogeneous optic axis orientation. This model works equally for biaxial media once one fixes the propagation direction of the transmitted light. In such a case, there are still two (effective) refractive indexes associated with specific orthogonal polarizations, which can be calculated by knowing the wavevector of the incident beam and the orientation of the index ellipsoid (see e.g. [31]). In the following, we conventionally define as "optic axis" the axis corresponding to the highest refractive index experienced by the incident light beam. Assuming the sample is sufficiently thin and lying in the plane $z = 0$, we have an optic axis angle θ which is a function of the azimuthal angle and radius in cylindrical coordinates: $\theta(\rho, \phi)$. The action of an anisotropic uniaxial medium can be expressed by the following Jones matrix, written in circular polarization basis:

$$U(\delta, \theta) = \cos\left(\frac{\delta}{2}\right)\begin{bmatrix}1 & 0\\ 0 & 1\end{bmatrix} + i\,\sin\left(\frac{\delta}{2}\right)\begin{bmatrix}0 & \mathrm{e}^{-2i\theta}\\ \mathrm{e}^{2i\theta} & 0\end{bmatrix}, \quad (1)$$

where the parameter δ is the optical retardation of the medium, $\delta = 2\pi(n_1 - n_2)d/\lambda$, with $n_{1,2}$ the two effective refractive indices, d the sample thickness and λ the wavelength. Note that δ can be position dependent as well, and in particular, in the case of banded "maltese-cross"-like patterns.

At half-wave retardation $\delta = \pi$, the effect of such a medium is to invert the handedness of circular polarisation and introduce a phase factor $\exp(\pm i2\theta(\rho, \phi))$, where the $+$sign is in the case of input left circular polarisation, and the $-$sign for input right circular polarisation. In particular, media characterized by the optic axis angle anisotropy

$$\theta_q(\rho, \phi) = q\phi + \theta_0, \quad (2)$$

where q is the topological charge of the molecular director field and θ_0 an offset angle, introduce azimuthal phase factors of $\exp(\pm i2\theta_0)\exp(\pm i2q\phi)$. Beams characterized by $\exp(i\ell\phi)$ factors are known for carrying a well-defined amount of OAM equal to $N\hbar\ell$ (where N is the average number of photons). Therefore, the medium described by $U(\pi, \theta_q)$ is converting the input spin angular momentum (SAM) of each input photon into OAM, a process known as SAM-to-OAM conversion (STOC), first investigated with q-plates [4]. Moreover, an input beam that is linearly polarized (or in a generic elliptical polarisation state) will be transformed into a non-separable state of polarisation and OAM, which manifests in inhomogeneous polarisation patterns [32, 33].

To test that our samples of ascorbic acid spherulites have a local optic axis around defects of $\theta = \phi$, we observed both the STOC phenomenon and the generation of inhomogeneous polarisation patterns.

3.1 Experimental characterization of the optic axis pattern

We first confirmed that the ascorbic acid crystals orient radially by measuring the optic axis pattern $\theta := \theta(\rho, \phi)$. This can be done by shining the sample with circular polarisation and projecting the transmitted beam into a linear polarisation state. The resulting intensity distribution is given by

$$I(\rho, \phi) \propto 1 + \sin(\delta)\sin(2\theta(\rho, \phi)), \quad (3)$$

where we assumed input right-circular polarisation and a projection on horizontal polarisation. The measurement was performed with a 633 nm diode laser source. At this wavelength our sample exhibits a retardation close to $\delta = \pi/2$, ensuring a good visibility of the intensity modulation in the measured pattern. As shown in Figure 3(B), near point defects, the recorded intensity distribution (averaged over different radial positions) is well described by the relation $\theta = \phi$, associated with a radial distribution of the molecular director around the defect. In proximity of boundaries

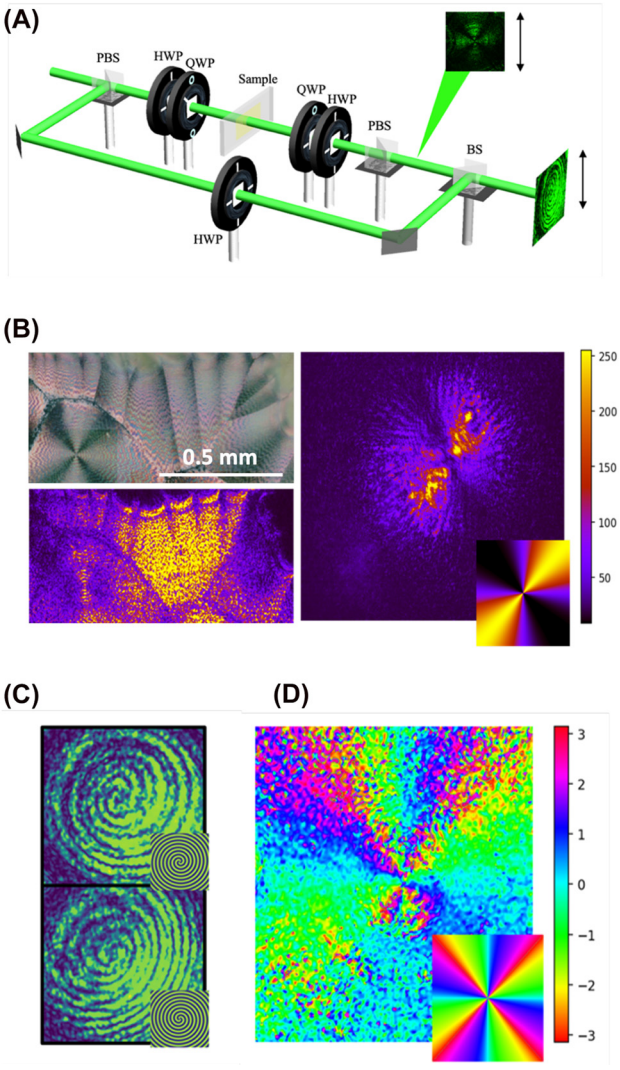

Figure 3: Structured light emerging from ascorbic acid spherulites. (A) Schematics of the interferometry and polarimetry setups. The reference beam's polarization is rotated in the reference arm to ensure non-orthogonal polarizations at the output of the BS. A lens (not shown) is also added to the reference arm to induce a spherical wavefront onto the reference Gaussian beam. For polarization tomography, the reference beam is ignored and the camera is placed between the PBS and the BS, as shown. (B) Intensity patterns characterizing the optic axis angle in two different regions of the sample. Right-circular polarization is incident on the sample and projected onto horizontal polarization, resulting in an intensity distribution related to the optic axis angle by 3. On the right, the distribution around a defect. It matches the simulated intensity for $\theta = \phi$, shown in the bottom right corner. On the bottom left, the intensity distribution of the image above, showing a region near a physical boundary. The intensity does not vary in that region. (C) On top, interference pattern generated with input right circular polarization, compared to the theoretical pattern between a spherical Gaussian and a beam carrying OAM +2. On the bottom, interference pattern generated with input left circular polarization, compared to the theoretical pattern between a spherical Gaussian and a beam carrying OAM -2. (D) Density plot of the major axes of the point-by-point polarization ellipses from a beam transmitted through a defect region of the sample. The V-point is visible. A simulation of the expected density plot is shown in the bottom right corner.

which separate regions containing point defects, we observe a jump in the optic axis angle.

3.2 STOC in ascorbic acid samples

A simple way to ascertain the generation of OAM in a laser beam is to look at its interference with a reference Gaussian beam [4]. It is easy to show that, in the case of co-propagating beams, the interference pattern consists of spiral fringes where the number of arms is dictated by the OAM absolute value of the analyzed beam, and the handedness by the OAM sign (see insets in Figure 3(C) for simulations). We thus verified this result by inserting the samples in one arm of an interferometer and recording the interference pattern for right-handed and left-handed circular polarisation inputs (the experimental setup is shown in Figure 3(A)). We used a laser beam at 525 nm, where the optical retardation of the samples is typically close to π. This was checked by looking at the conversion efficiency from left circular to right circular polarization [5].

The resulting interference patterns are shown in Figure 3(C) for right and left circular polarisations, respectively, showing that the STOC phenomenon is realized.

3.3 Polarimetry of vector modes

As the next step we illuminated the sample with the same laser beam but with linear polarisation. The q-plate model predicts that the resulting field, on the sample plane and at half-wave retardation, is given by

$$\mathbf{E}_{\text{out}}(\rho, \phi) \propto \left(e^{i2\phi}\mathbf{e}_R + e^{-i2\phi}\mathbf{e}_L\right)e^{-\rho^2/w^2}, \tag{4}$$

where we assumed a Gaussian envelope field with waist w, and $\mathbf{e}_{R,L} = (\mathbf{x} \pm i\mathbf{y})/\sqrt{2}$, with $\mathbf{x}$ and $\mathbf{y}$ the unit vectors of the x and y axes. Such a field is linearly polarised everywhere but with an angle of the polarisation ellipse given by ϕ and a singular point on the beam axis (known as a "V"-point) [33]. A detailed account of polarization singularities emerging from biaxial media is given in Ref. [34]. We observed the generation of these patterns by a point-by-point measurement of the Stokes parameters, defined by: $s_0 = I_{\text{total}}, s_1 = I_H - I_V, s_2 = I_A - I_D, s_3 = I_L - I_R$, where $I_{H,V,A,D,L,R}$ are the intensities of, respectively, horizontal, vertical, anti-diagonal, diagonal, left circular and right circular polarisation, and I_{total} stands for total intensity. These intensities, and consequently the Stokes parameters, can all be easily measured by a sequence containing a quarter-wave plate, a half-wave plate and a polarizing beam splitter (Figure 3(A)). In particular, the density plot of the

polarisation ellipse orientation (which is the phase of the field $s_1 + is_2$) clearly shows a singular pattern (Figure 2(D)). By according the different projection intensities on a camera, we reconstructed the local polarisation ellipse. The resulting pattern is quantitatively close to the expected one. Due to the optical retardation not being exactly π, the "V"-point is split in four points of circular polarisation ("C"-points) each with a topological charge 1/2 (see also ref. [33]).

The generation of singular polarization patterns was observed also during the growth of the sample (Figure 4). Figure 4 shows how the radial pattern appears first around the defect and then spreads through the sample.

4 Discussion

We have shown that ascorbic acid spherulites crystallize around defects, in the absence of twisting, with a local optic axis pattern of $\theta = \phi$. We have also shown experimentally the generation of OAM modes and vector beams. Our findings show how ascorbic acid can be exploited as a material for fabricating devices which exploit photonic spin–orbit phenomena. In future, we plan to develop techniques to better control the growth of the ascorbic acid samples in ways analogous to what is done with liquid crystals [5].

The radial growth around the defect is likely the most energetically efficient way to form the hydrogen bonds between atoms inside the crystal. It can be interesting to explore the different crystallization structures when ascorbic acid is grown on a polar substrate, instead of around a defect on a neutral glass substrate.

Ascorbic acid is part of a large family of spherulites, each of which has structures suggesting certain anisotropy of optic axis patterns around defects. It would be interesting to explore the STOC phenomena in other kinds of spherulites, which may have advantages over ascorbic acid. In particular, while ascorbic acid has relevant absorption above 1.5 THz [35], the recently demonstrated controlled generation of quartz spherulites [36, 37] may offer an interesting way for creating vortex beams in the TeraHertz frequency domain [38] (q plates for this regime have been recently realized using either 3D printing techniques [39] or quartz segmented waveplates [40]). It would also shed light on the role of different crystal structures and symmetries in the shaping of light.

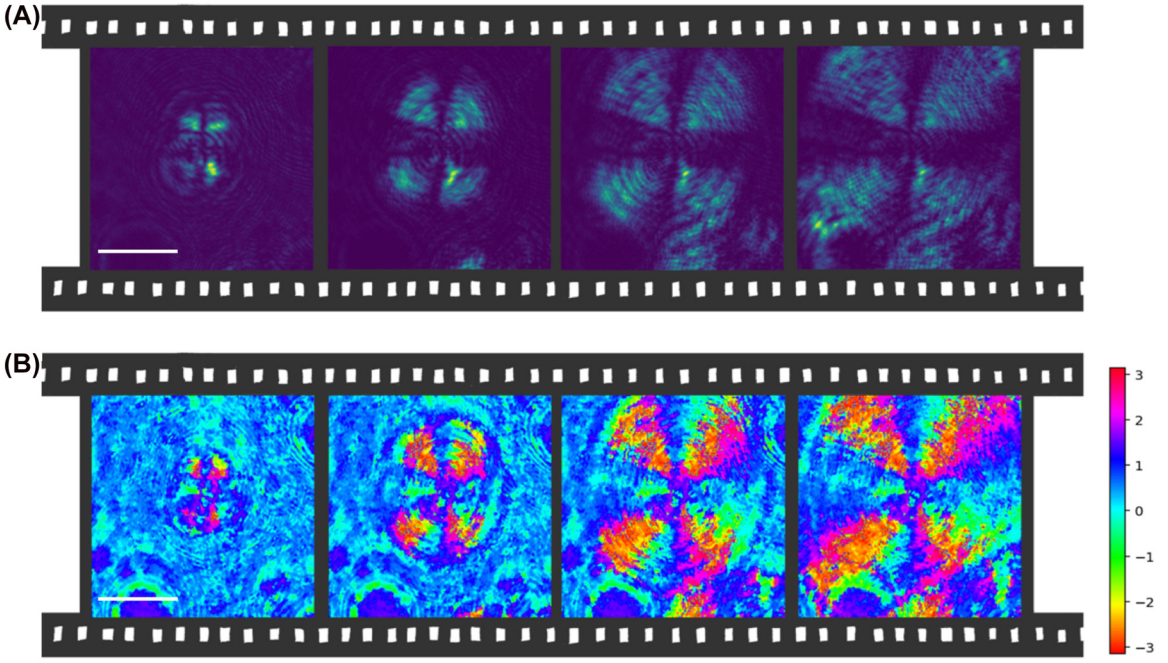

Figure 4: Frames showing the evolution of polarization distribution during the growth of the sample at $t = 0$ min, 6.5 min, 12.8 min, 19.1 min. The sample was grown at room temperature, from a solution of 10:1 ethanol:water. (A) Intensity of the beam between cross polarizers at different times during crystal growth. (B) Plot of the major axis angle of the point-by-point polarization ellipses at different times during crystal growth.

Author contributions: All the authors have accepted responsibility for the entire content of this submitted manuscript and approved submission.
Research funding: This work was supported by the Canada Research Chairs (CRC) and Canada First Research Excellence Fund (CFREF) Program, and Joint Centre for Extreme Photonics (JCEP).
Conflict of interest statement: The authors declare no conflicts of interest regarding this article.

References

[1] B. Crist and J. M. Schultz, "Polymer spherulites: a critical review," *Prog. Sci. Polym.*, vol. 56, p. 1, 2016.
[2] L. Marrucci, C. Manzo, and D. Paparo, "Pancharatnam-berry phase optical elements for wave front shaping in the visible domain: switchable helical mode generation," *Appl. Phys. Lett.*, vol. 88, p. 221102, 2006.
[3] G. Biener, A. Niv, V. Kleiner, and E. Hasman, "Formation of helical beams by use of pancharatnam—berry phase optical elements," *Opt. Lett.*, vol. 27, p. 1875, 2002.
[4] L. Marrucci, C. Manzo, and D. Paparo, "Optical spin-to-orbital angular momentum conversion in inhomogeneous anisotropic media," *Phys. Rev. Lett.*, vol. 96, p. 163905, 2006.
[5] A. Rubano, F. Cardano, B. Piccirillo, and L. Marrucci, "Q-plate technology: a progress review," *JOSA B*, vol. 36, p. D70, 2019.
[6] E. Nagali, F. Sciarrino, F. De Martini, et al., "Quantum information transfer from spin to orbital angular momentum of photons," *Phys. Rev. Lett.*, vol. 103, p. 013601, 2009.
[7] F. Cardano, E. Karimi, L. Marrucci, C. de Lisio, and E. Santamato, "Generation and dynamics of optical beams with polarization singularities," *Opt. Express*, vol. 21, p. 8815, 2013.
[8] L. Yan, P. Gregg, E. Karimi, et al., "Q-plate enabled spectrally diverse orbital-angular-momentum conversion for stimulated emission depletion microscopy," *Optica*, vol. 2, p. 900, 2015.
[9] E. Karimi, B. Piccirillo, E. Nagali, L. Marrucci, and E. Santamato, "Efficient generation and sorting of orbital angular momentum eigenmodes of light by thermally tuned q-plates," *Appl. Phys. Lett.*, vol. 94, p. 231124, 2009.
[10] J. J. J. Nivas, S. He, A. Rubano, et al., "Direct femtosecond laser surface structuring with optical vortex beams generated by a q-plate," *Sci. Rep.*, vol. 5, p. 1, 2015.
[11] B. Piccirillo, V. D'Ambrosio, S. Slussarenko, L. Marrucci, and E. Santamato, "Photon spin-to-orbital angular momentum conversion via an electrically tunable q-plate," *Appl. Lett.*, vol. 97, p. 4085, 2010, arXiv:1010.4473.
[12] M. Beresna, M. Gecevičius, P. G. Kazansky, and T. Gertus, "Radially polarized optical vortex converter created by femtosecond laser nanostructuring of glass," *Appl. Phys. Lett.*, vol. 98, p. 201101, 2011.
[13] E. Karimi, S. A. Schulz, I. De Leon, H. Qassim, J. Upham, and R. W. Boyd, "Generating optical orbital angular momentum at visible wavelengths using a plasmonic metasurface," *Light: Sci. Appl.*, vol. 3, p. e167, 2014.
[14] A. Kavokin, G. Malpuech, and M. Glazov, "Optical spin hall effect," *Phys. Rev. Lett.*, vol. 95, p. 136601, 2005.
[15] N. C. Zambon, P. St-Jean, M. Milićević, et al., "Optically controlling the emission chirality of microlasers," *Nat. Photonics*, vol. 13, p. 283, 2019.
[16] V. D'Ambrosio, E. Nagali, S. P. Walborn, et al., "Complete experimental toolbox for alignment-free quantum communication," *Nat. Commun.*, vol. 3, p. 961, 2012.
[17] R. Fickler, R. Lapkiewicz, W. N. Plick, et al., "Quantum entanglement of high angular momenta," *Science*, vol. 338, p. 640, 2012.
[18] G. Vallone, V. D'Ambrosio, A. Sponselli, et al., "Free-space quantum key distribution by rotation-invariant twisted photons," *Phys. Rev. Lett.*, vol. 113, p. 060503, 2014.
[19] A. E. Willner, Y. Ren, G. Xie, et al., "Recent advances in high-capacity free-space optical and radio-frequency communications," *Philos. Trans. R. Soc., A*, vol. 375, p. 20150439, 2017.
[20] A. Sit, R. Fickler, F. Alsaiari, et al., "Quantum cryptography with structured photons through a vortex fiber," *Opt. Lett.*, vol. 43, p. 4108, 2018.
[21] K. Yu Bliokh and Y. P. Bliokh, "Conservation of angular momentum, transverse shift, and spin hall effect in reflection and refraction of an electromagnetic wave packet," *Phys. Rev. Lett.*, vol. 96, p. 073903, 2006.
[22] S. Liu, S. Chen, S. Wen, and H. Luo, "Photonic spin hall effect: fundamentals and emergent applications," *Opto-Electron. Sci.*, vol. 1, p. 220007, 2022.
[23] E. G. Cox, "Crystalline structure of hexuronic acid," *Nature*, vol. 130, p. 205, 1932.
[24] J. Hvoslef, "The crystal structure of l-ascorbic acid, 'vitamin c'. i. the x-ray analysis," *Acta Crystallogr. Sect. B: Struct. Crystallogr. Cryst. Chem.*, vol. 24, p. 23, 1968.
[25] H. Uesaka and R. Kobayashi, "Pattern formation in the crystallization of ascorbic acid," *J. Cryst. Growth*, vol. 237, p. 132, 2002.
[26] W. Omar, *Effect of Solvent Composition on Cristallization Process of Ascorbic Acid*, vol. 29, Weinheim, Chemical Engineering & Technology: Industrial Chemistry-Plant Equipment-Process Engineering-Biotechnology, 2006. Available at: https://doi.org/10.1002/ceat.200500283.
[27] Y. Yamazaki, H. Yoshino, M. Izui, Y. Sato, and M. Matsushita, "Humidity—"temperature dependence of domain growth of ascorbic acid crystal"," *J. Phys. Soc. Jpn.*, vol. 78, p. 074001, 2009.
[28] S. K. Kon and M. B. Watson, "The effect of light on the vitamin c of milk," *Biochem. J.*, vol. 30, p. 2273, 1936.
[29] M. Ito, M. Izui, and M. Matsushita, "Morphological diversity in crystal growth of l-ascorbic acid dissolved in methanol," *J. Phys. Soc. Jpn.*, vol. 72, p. 1834, 2003.
[30] F. P. Price, "The structure of high polymer sperulites," *J. Polym. Sci.*, vol. 37, p. 71, 1959.
[31] B. E. A. Saleh and M. C. Teich, *Fundamentals of Photonics*, Hoboken, New Jersey, John Wiley & Sons, 2019.
[32] F. Cardano, E. Karimi, S. Slusarenko, L. Marrucci, E. Santamato, and C. de Lisio, "Polarisation pattern of vector vortex beams generated by q-plates with different topological charges," *Appl. Opt.*, vol. 52, p. C1, 2012.
[33] A. D'Errico, M. Maffei, B. Piccirillo, C. de Lisio, F. Cardano, and L. Marrucci, "Topological features of vector vortex beams

perturbed with uniformly polarized light," *Sci. Rep.*, vol. 7, p. 1, 2017.

[34] M. V. Berry and M. R. Dennis, "The optical singularities of birefringent dichroic chiral crystals," *Proc. R. Soc. London, Ser. A*, vol. 459, p. 1261, 2003.

[35] L. Jiang, M. Li, C. Li, et al., "Terahertz spectra of l-ascorbic acid and thiamine hydrochloride studied by terahertz spectroscopy and density functional theory," *J. Infrared, Millimeter, Terahertz Waves*, vol. 35, p. 871, 2014.

[36] S. Zhou, J. Antoja-Lleonart, P. Nukala, V. Ocelik, N. R. Lutjes, and B. Noheda, "Crystallization of geo2 thin films into alpha-quartz: from spherulites to single crystals," *Acta Mater.*, vol. 215, p. 117069, 2021.

[37] N. R. Lutjes, S. Zhou, J. Antoja-Lleonart, B. Noheda, and V. Ocelík, "Spherulitic and rotational crystal growth of quartz thin films," *Sci. Rep.*, vol. 11, p. 1, 2021.

[38] H. Wang, Q. Song, Y. Cai, et al., "Recent advances in generation of terahertz vortex beams and applications," *Chin. Phys. B*, vol. 29, p. 097404, 2020.

[39] A. I. Hernandez-Serrano, E. Castro-Camus, and D. Lopez-Mago, "q-plate for the generation of terahertz cylindrical vector beams fabricated by 3d printing," *J. Infrared, Millimeter, Terahertz Waves*, vol. 38, p. 938, 2017.

[40] A. Minasyan, C. Trovato, J. Degert, E. Freysz, E. Brasselet, and E. Abraham, "Geometric phase shaping of terahertz vortex beams," *Opt. Lett.*, vol. 42, p. 41, 2017.